https://doi.org/10.5194/egusphere-2023-1215
Preprint. Discussion started: 10 July 2023

Oxygenated organic molecules produced by low-NO_x photooxidation of aromatic compounds and their contributions to secondary organic aerosol

Xi Cheng[1], Yong Jie Li[2], Yan Zheng[1], Keren Liao[1], Tong Zhu[1], Chunxiang Ye[1], Xinghua Qiu[1], Theodore K. Koenig[1], Yanli Ge[1], Qi Chen[1]

[1]State Key Joint Laboratory of Environmental Simulation and Pollution Control, BIC-ESAT and IJRC, College of Environmental Sciences and Engineering, Peking University, Beijing, China

[2]Department of Civil and Environmental Engineering, Department of Ocean Science and Technology, and Centre for Regional Oceans, Faculty of Science and Technology, University of Macau, Taipa, Macau, China

Correspondence: Qi Chen (qichenpku@pku.edu.cn) and Yong Jie Li (yongjieli@um.edu.mo)

https://doi.org/10.5194/egusphere-2023-1215
Preprint. Discussion started: 10 July 2023

Abstract. Oxygenated organic molecules (OOMs) produced by the oxidation of aromatic compounds are key components of secondary organic aerosol (SOA) in urban environments. The steric effects of substitutions and rings and the role of key reaction pathways on altering the OOM distributions remain unclear because of the lack of systematic multi-precursor study over a wide range of OH exposure. In this study, we conducted flow-tube experiments and used the nitrate adduct time-of-flight chemical ionization mass spectrometer (NO_3^--TOF-CIMS) to measure the OOMs produced by the photooxidation of six key aromatic precursors under low-NO_x conditions. For single aromatic precursors, the detected OOM peak clusters show one or two oxygen-atom difference, indicating the involvement of multi-step auto-oxidation and alkoxy radical pathways. Multi-generation OH oxidation is also needed to explain the diverse hydrogen numbers in the observed formulae. Especially for double-ring precursors at higher OH exposure, multi-generation OH oxidation may have significantly enriched the dimer formulae. Methyl substitutions in precursor may lead to less fragmented products in the OOMs, while the double-ring structure corresponds to less efficient formation of closed-shell monomeric and dimeric products, both highlighting significant steric effects of precursor molecular structure on the OOM formation. The estimated accretion reaction rate constants for key dimers formed from the benzene oxidation are much greater than those formed from the naphthalene oxidation (7.0 vs. 0.9×10^{-10} cm^3 $molecules^{-1}$ s^{-1}). Naphthalene-derived OOMs however have lower volatilities and greater SOA contributions than the other-types of OOMs, which may be more important in initial particle growth. Overall, the OOMs identified by the NO_3^--TOF-CIMS perhaps consist of 3-11% of the SOA mass. Our results highlight the key roles of progressive OH oxidation, methyl substitution and ring structure in the OOM formation from aromatic precursors, which needs to be considered in future model developments to improve the model performance on organic aerosol.

https://doi.org/10.5194/egusphere-2023-1215
Preprint. Discussion started: 10 July 2023

1 Introduction

Oxidation of volatile organic compounds (VOCs) leads to the formation of ozone and secondary organic aerosols (SOA) (Ziemann and Atkinson, 2012). Light and heavy aromatic VOCs are important SOA precursors that can be emitted from various anthropogenic sources such as transportation, solvent use, wood burning, coal burning, and cooking (Henze et al., 2008; Pye and Pouliot, 2012). There are many chamber studies on the SOA formation from aromatic VOCs (Li et al., 2016a; Li et al., 2016b; Lambe et al., 2011; Ng et al., 2007; Chan et al., 2009; Kautzman et al., 2010). The derived SOA yields vary by precursors and NO_x levels owing to the difference in forming condensable products, i.e., oxygenated organic molecules (OOMs). Characterization of these OOM species is however limited and challenging. Most of atmospheric chemical transport models (CTM) still use SOA-yield-based parameterizations, which have difficulties in reproducing the concentration and the variability of organic aerosol in urban areas (Tsigaridis et al., 2014).

Recent developments in time-of-flight chemical ionization mass spectrometry provide new insights into the formation of OOMs and their contribution to SOA (Bianchi et al., 2019). Wang et al. (2017) indicate that intramolecular H-shift of peroxy radicals (RO_2) from alkyl benzenes can compete with bimolecular reactions under atmospheric conditions, thereby substantially increasing the product oxygen numbers via auto-oxidation. Laboratory studies show further evidence for the occurrence of both of multi-generation OH oxidation and multi-step auto-oxidation in the aromatic oxidation to increase the oxidation state of the products (Garmash et al., 2020; Cheng et al., 2021b). Berndt et al. (2018b) suggest high formation rates of accretion products from self- and cross-reactions of RO_2 radicals for aromatic precursors, resulting in great carbon and oxygen number increments that lower the product volatility. The three mechanisms, i.e., multi-generation OH oxidation, multi-step auto-oxidation, and accretion reactions, play different roles under different oxidation conditions. Aromatic precursors also differ in substituents and ring numbers, which may cause steric effects in the OOM formation. Cheng et al. (2021b) suggest that for benzene and toluene, the multi-generation OH oxidation likely proceeds more favorably by H subtraction than OH addition and the dimer formation is unfavorable at high OH exposures. Other laboratory studies indicate that under similar OH exposures, the oxidation of isopropylbenzene, ethylbenzene and toluene likely forms more oxidized RO_2 radicals than the oxidation of benzene does (Wang et al., 2017). Moreover, the formation of dimeric products from the oxidation of trimethylbenzene may be more significant for meta-substituents than for ortho-substituents (Wang et al., 2020). However, there is still a lack of multi-precursor studies that compares the OOM formations systematically under a wide range of OH exposure. A better understanding of the precursor steric effects and the OOM potential of forming SOA is needed to assist future developments of more detailed model representation on the SOA formation.

Herein, the formation of OOMs from six aromatic VOCs (i.e., benzene, toluene, m-xylene, 1,3,5-trimethylbenzene, naphthalene, and 1-methylnaphthalene) is investigated in the flow-tube experiments under low-NO_x conditions, aiming at gaining insights into the OH-initiated chemistry and the low-NO_x representation of suburban and downwind environments. The OOMs are characterized by using a nitrate adduct time-of-flight chemical ionization mass spectrometer (NO_3^--TOF-CIMS). The experiments cover a wide range of OH exposures that are equivalent to approximately 1 - 19 days assuming a

https://doi.org/10.5194/egusphere-2023-1215
Preprint. Discussion started: 10 July 2023

mean OH concentration of 1.5×10^6 molecules cm^{-3}. The influences of precursor structure and OH exposure on the formation of OOMs and the contributions of the identified OOMs to SOA are investigated.

2 Methods

2.1 Experimental procedures

Experiments were conducted in a 13.3-L Aerodyne oxidation flow reactor (OFR) with a mean residence time of 95 s under low-NO_x conditions. The operation of the OFR has been described previously by Cheng et al. (2021b). The OFR was operated in an OFR254-5 mode, with 254 nm lights on and 5 ppm of externally generated O_3 introduced into the OFR (Lambe et al., 2017; Peng et al., 2018). The OH radicals are generated via:

$$O_3 + h\nu\ (254\ nm) \rightarrow O_2 + O(^1D) \quad (R1)$$

$$O(^1D) + H_2O \rightarrow 2OH \quad (R2)$$

The relative humidity (RH) inside the OFR was maintained at 23.4 - 29.4%. Concentrations of OH radicals were varied by ramping the voltage of the UV lamps in the OFR, for which each lamp voltage represents one experimental condition. All experiments herein were conducted without NO_x injection. We estimate a background NO_x level of < 1 ppb throughout the experiments. In total, 27 experiments were performed for the six aromatic precursors. Table 1 lists the experimental conditions and the key measured and derived quantities, including those for the oxidation of benzene and toluene that have been discussed in our previous study (Cheng et al., 2021b). The concentrations of OH and HO_2 radicals were estimated by using a photochemical box model (PAMchem) (Lambe et al., 2017; Cheng et al., 2021b). The results suggest that the first step of oxidation of the aromatic VOCs was dominated by the OH radicals rather than by O_3 because of much higher reaction rate constants for the former than the latter (Lambe et al., 2017; Peng et al., 2016). The reaction rates of early-generation oxidation products that contain double bounds with O_3 are also likely slower than those with OH radicals (Molteni et al., 2018; Wang et al., 2020). Therefore, we believe that the oxidation chemistry was prevalently initiated by OH radicals in our experiments.

2.2 Measurements

The concentration of O_3 was monitored with an UV photometric analyzer (2B Technologies, 202). Concentrations of aromatic VOCs were measured by an IONICON proton transfer reaction-quadrupole interface time-of-flight mass spectrometer (PTR-QiTOF). Calibration of PTR-QiToF was conducted by using gas standards (Spectra Gases, ~1 ppm) at different concentration levels. The measurements uncertainty is about 15% for calibrated species (Huang et al., 2019). Particle size distributions were measured by a scanning mobility particle sizer (SMPS; TSI, 3938). The SOA mass concentrations were measured by an Aerodyne long time-of-flight soot particle aerosol mass spectrometer (LTOF-SP-AMS). Calibrations of ionization efficiency (IE) and relative IE (RIE) followed the standard procedures by using pure ammonium

https://doi.org/10.5194/egusphere-2023-1215
Preprint. Discussion started: 10 July 2023

nitrate (NH_4NO_3) and ammonium sulfate ($(NH_4)_2SO_4$) (Zheng et al., 2020). A collection efficiency (CE) value of 1 was applied to the LTOF-SP-AMS data herein. The oxygen-to-carbon (O:C) and hydrogen-to-carbon (H:C) ratios of SOA were estimated by the method introduced by Aiken et al. (2008). Because the measured ratios of $(H_2O^+)_{org}/(CO_2^+)_{org}$ (i.e., around 0.33) and $(CO^+)_{org}/(CO_2^+)_{org}$ (i.e., 1.1-1.2) for chamber aromatic SOA were similar to the default ratios of 0.225 and 1, respectively (Chhabra et al., 2011; Nakao et al., 2013), we did not update those ratios in the calculation of elemental ratios (Chen et al., 2011). The OOMs were measured by the Aerodyne NO_3^--TOF-CIMS in the form of deprotonated ions, clusters with a nitrate monomer, or clusters with a nitrate dimer. This study only presents clusters having one nitrate ion (Cheng et al., 2021b). The background signals of individual OOMs were determined from measurements made without the injection of VOC precursors. A calibration factor of 1.66×10^{10} molecules cm^{-3} was applied to all OOMs when converting their signals to concentrations, with an estimated uncertainty of 42%. The instrument operation and data analysis have been described in detail in our previous studies (Cheng et al., 2021a; Cheng et al., 2021b).

2.3 Dimer formation rates

Dimeric products may be formed by the accretion reactions between RO_2 and $R'O_2$ radicals. At steady state, the formation rate of dimers is represented as follows:

$$\frac{d[ROOR']}{dt} = \sum_i^n k_{R,i}[RO_2][R'O_2] - k_{loss}[ROOR'] = 0 \quad (1)$$

where $k_{R,i}$ (cm^3 $molecule^{-1}$ s^{-1}) is the apparent rate constants of accretion reactions ($i \geq 1$), and k_{loss} (s^{-1}) represents the loss rate of OOMs (0.04-0.1 s^{-1}) (Cheng et al., 2021b). At the exit of the OFR, the OOMs that form slowly would not be detectable by the NO_3^--TOF-CIMS because of the fast vapor losses. The detected dimeric products often show rapid increases to stable concentrations in their time series, suggesting fast formation rates (Figure S1). We use Eq. 1 to provide rough constraints to the formation rate constants of detected dimeric products, which is similar to the approach used by Molteni et al. (2019). There are 46, 54, and 76 assigned dimeric products from benzene, toluene, and naphthalene experiments, respectively, from the NO_3^--TOF-CIMS measurements of OOM molecular formulae. However, for each precursor, only 5-8 dimers have sufficient combinations of above-detection-limit signals of possible RO_2 and $R'O_2$ to solve $k_{R,i}$ by using a non-negative multi-linear regression method (Sklearn from Python 3). Only the $k_{R,i}$ values that are greater than zero but less than 9×10^{-10} cm^3 $molecule^{-1}$ s^{-1} (considering the collision limit) with correlation coefficients (r) of > 0.5 are considered as reasonable rate constants and are listed in Table 2.

2.4 Condensation estimation

The contributions of the detected OOMs to SOA were only estimated for benzene, toluene, and naphthalene experiments, for which both LTOF-SP-AMS and SMPS measurements are available. We consider both irreversible and equilibrium-type condensation. The former was represented by the net condensation flux of the observed OOMs, which is described by using an aerosol growth model (Tröstl et al., 2016). The latter was represented by the particulate fraction estimated with the

https://doi.org/10.5194/egusphere-2023-1215
Preprint. Discussion started: 10 July 2023

partitioning theory and the vapor pressure of OOMs (Pankow, 1994). An empirical volatility parameterization was used to estimate the saturation concentrations (C^*) of the detected OOMs (Mohr et al., 2019). The OOMs were grouped into volatility bins based on the volatility-basis-set (VBS) method (Donahue et al., 2006). Specifically, they were classified as ultralow volatility organic compounds (ULVOC, $\log C^* \leq -9.5$), extremely low volatility organic compounds (ELVOC, $-9.5 < \log C^* \leq -4.5$), low volatility organic compounds (LVOC, $-4.5 < \log C^* \leq -0.5$), semi-volatile organic compounds (SVOC, $-0.5 < \log C^* \leq 2.5$), and intermediate volatility organic compounds (IVOC, $2.5 < \log C^* \leq 6.5$) (Bianchi et al., 2019; Schervish and Donahue, 2020). In this study, SOA contributions from OOMs with C^* of ≤ 0.01 μg m^{-3} were calculated by the aerosol growth model, and those from OOMs with $C^* > 0.01$ μg m^{-3} were calculated by the partitioning method. The calculation details are provided in Section S1 of the Supplement.

3 Results and discussion

3.1 Product distributions

The general oxidation chemistry for OH-initiated pathways of aromatic VOCs is described in Section S2 of the Supplement. Figure 1 shows the OOM product distributions for the oxidation of the six aromatic precursors under similar OH exposures of approximately $(1.2\text{-}1.5)\times10^{12}$ molecules cm^{-3} s. For a given precursor of C_xH_y, we name the detected OOMs as monomeric products ($C_{<x}$ and C_x series) and dimeric products ($C_{<2x}$ and C_{2x} series). Monomeric products contribute to the majority of the detected OOM signals for the six aromatic precursors studied herein, while the dimeric products contribute to up to 18% of the OOM signals. The highest dimeric signal fraction is observed for m-xylene OOMs. Overall, ion peaks in the mass-to-charge (m/z) range of 200-650 Thomson (Th) show in clusters with progressions and sequences that preserve the precursor carbon structure. The lower ends of the peak clusters of monomeric products for benzene, toluene, m-xylene, and 1,3,5-trimethylbenzene are shifted by progressive differences of 14 Th ($-CH_2$). The products from naphthalene and 1-methylnaphthalene also show a similar $-CH_2$ progression. The progression is doubled for dimeric products (28 Th, $-(CH_2)_2$). Moreover, there are series of clusters with peak sequences that differ by one and two oxygen atoms in both of monomeric and dimeric products, respectively, in each mass spectrum. The peak clusters then differ by hydrogen atom numbers for each oxygen atom addition. The general shifting of peak abundance to products with 1-4 more hydrogen (i.e., to the right m/z side) is consistent with the importance of OH addition in the oxidation of aromatic precursors. By contrast, dimeric clusters show more abundant distributions in the hydrogen-deficient m/z values (i.e., on the left side), suggesting significant hydrogen loss in the dimer formation.

The $C_{<x}$ products are typically fragmented products formed from the decomposition of alkoxy (RO) radicals (Li and Wang, 2014). Methyl substitution may prevent the efficient formation of phenoxy radicals, thereby lowering the abundance of fragmented products (Schwantes et al., 2017). Indeed, we observed high signal fractions of $C_{<x}$ products (59.4-65.7%) in OOMs produced by the oxidation of benzene, toluene, naphthalene and 1-methylnaphthalene that have low methyl-to-aryl

https://doi.org/10.5194/egusphere-2023-1215
Preprint. Discussion started: 10 July 2023

carbon ratios (C_{Me}:C_{Ar} < 0.2), whereas the signal fractions of $C_{<x}$ products produced by the oxidation of m-xylene and 1,3,5-trimethylbenzene (C_{Me}:C_{Ar} > 0.2) are much lower (17.9-26.3%). Tables S1-S6 in the Supplement list the formulae and the relative signals of major OOMs for the experiments presented in Figure 1. For the oxidation of benzene, toluene, naphthalene and 1-methylnaphthalene, $C_3H_4O_5$ and $C_4H_4O_5$ are the main common $C_{<x}$ products. These molecules are likely second- or third-generation products formed via the fragmentation of phenoxy radicals with rich unsaturated aryl carbon moieties (Schwantes et al., 2017). $C_5H_6O_6$ and $C_8H_{10}O_7$ are the most abundant $C_{<x}$ products for the oxidation of m-xylene and 1,3,5-trimethylbenzene, respectively. $C_5H_6O_6$ is likely a ring-scission product (e.g., carboxylic acid), while $C_8H_{10}O_7$ may be a fragmented ring-retaining product formed by the dealkylation pathway (Zaytsev et al., 2019; Mehra et al., 2020).

The C_x products with odd H numbers in their formulae for single-precursor oxidation systems are plausibly open-shell products (i.e., mainly RO_2) (Zhao et al., 2018), and the C_x products with even H numbers are normally closed-shell neutrals. Central in the formation of OOMs from aromatic VOCs, the bicyclic peroxy radicals (BPRs) contain 5 oxygen numbers ($C_xH_{y+1}O_5$), which are formed by two steps of O_2 addition after OH addition (Birdsall et al., 2010). As shown in Table S7, the signal fractions of $C_xH_{y+1}O_7$ and $C_xH_{y+1}O_9$ (0.1-1.0%) are greater than those of $C_xH_{y+1}O_5$ (0.05-0.4%), explained by aggressive multiple steps of auto-oxidation. These odd-oxygen RO_2 radicals are the results of the predominant OH-addition plus sequential O_2 incorporation (auto-oxidation). Besides, even-oxygen RO_2 radicals are observed, with $C_xH_{y+1}O_6$ and $C_xH_{y+1}O_8$ (0.1-1.1%) being the most abundant, and their formation might involve the RO pathway (Orlando et al., 2003; Cheng et al., 2021b). In the RO pathway, the RO radicals undergo intermolecular H-shift (isomerization) instead of decomposition, which forms C-centered alkyl radicals that are ready for further auto-oxidation. For example, the BPR ($C_xH_{y+1}O_5$) can react with HO_2 to form the RO radical $C_xH_{y+1}O_4$. The newly formed RO radical then isomerizes to become a hydroxylated alkyl radical and results in a new RO_2 radical ($C_xH_{y+1}O_6$) via O_2 addition. The most abundant C_x neutrals are $C_6H_6O_6$ (3.1%), $C_7H_8O_6$ (3.8%), $C_8H_{10}O_7$ (8.6%), $C_9H_{14}O_7$ (17.5%), $C_{10}H_8O_6$ (2.9%), and $C_{11}H_{12}O_{10}$ (2.1%) for the oxidation of benzene, toluene, m-xylene, 1,3,5-trimethylbenzene, naphthalene and 1-methylnaphthalene, respectively. We obtained average O:C ratios of 0.9-1.1 for closed-shell OOM products formed from monocyclic precursors and 0.7-0.8 for those formed from double-ring precursors. The lower O:C ratios for the latter is probably because the second aromatic ring prohibits extensive auto-oxidation (Molteni et al., 2018).

For dimeric products, the C_{2x} products are much more abundant than the $C_{<2x}$ products in terms of both number and amount (Tables S1-S6). The observed C_{2x} dimers have odd and even oxygen numbers in their formulae, suggesting the occurrence of both of the cross- and self-reactions of RO_2 radicals. For example, $C_{18}H_{26}O_{12}$ is a product from the 1,3,5-trimethylbenzene oxidation, which may be formed via self-reactions of $C_9H_{13}O_7$ or cross-reactions of other even-oxygen RO_2 radicals. Interestingly, the C_{2x} products with 4-7 oxygen numbers show a greater abundance for the oxidation of m-xylene (Fig. 1c) than for those of other precursors, indicating more stable accretion products from less oxygenated RO_2 radicals derived from m-xylene due to stereoselectivity. Wang et al. (2020) also identified more abundant dimeric products for the meta-substitution precursor. Moreover, different numbers of hydrogen atoms in the dimer formulae suggest different formation

https://doi.org/10.5194/egusphere-2023-1215
Preprint. Discussion started: 10 July 2023

routes. For monocyclic aromatic precursors, the main C_{2x} products are $C_{2x}H_{2y+2}O_{10\text{-}14}$, likely formed by the accretion reactions of two $C_xH_{y+1}O_z$ radicals (Table S7). These $C_xH_{y+1}O_z$ are usually RO_2 radicals formed from multi-step auto-oxidation with one step of OH addition. Unlike the monocyclic precursors, the main C_{2x} products produced by the oxidation of naphthalene and 1-methylnaphthalene are $C_{2x}H_{2y}O_{10\text{-}14}$, $C_{2x}H_{2y+2}O_{10\text{-}14}$, and $C_{2x}H_{2y+4}O_{10\text{-}14}$, showing more diverse H number distributions. The result suggests more efficient multi-generation OH oxidation (e.g., adding one H atom via OH addition vs. losing one H atom via H abstraction) before accretion reactions occur for double-ring aromatic precursors.

The overall yields of the OOMs detected by the NO_3^--TOF-CIMS were calculated as $(k_{loss}\times[OOMs])/(k_1\times[VOC]\times[OH])$, where k_{loss} is the loss rate of OOMs and k_1 is the VOC-OH reaction rate coefficients. The AMS and SMPS particle measurements are only available for benzene, toluene, and naphthalene, for which we can correct the vapor loss of OOMs to the particle phase and the OFR wall (Cheng et al., 2021b). Figure 2 shows the OOM yields under different OH exposures. The yields range from 0.07% to 2.05%, among which the yields of naphthalene-derived OOMs are greater than those of the other two monocyclic aromatic precursors. This is consistent with the result from Molteni et al. (2018), which obtained a higher OOM yield for naphthalene (1.8%) than for benzene (0.2%) and toluene (0.1%). As the OH exposure increases, the OOM yields for benzene and toluene first increase and then decrease after the equivalent photochemical age exceeds 7 days. The initial increase of OOM yields is consistent with the results presented by Garmash et al. (2020) for the oxidation of benzene under low OH exposure. The later decrease of the apparent OOM yields under high OH exposure suggest the production of more fragmented products that remain undetected by the NO_3^--TOF-CIMS. For the oxidation of naphthalene, we find increasing OOM yields under high OH exposure. Multi-generation OH oxidation may occur more efficiently for precursors with two aromatic rings than the monocyclic precursors, thereby forming more of the detectable OOMs by the NO_3^--TOF-CIMS even under high OH exposure.

3.2 Formation of C_x and C_{2x} OOMs

For all precursors, the concentrations of closed-shell C_x products are much greater than those of open-shell products (i.e., mainly RO_2) (Figure S2). Under low-NO_x conditions, the closed-shell C_x products are formed primarily from the $RO_2 + HO_2$ pathways rather than the reaction of $RO_2 + RO_2$. This is due to the much higher HO_2 concentrations (0.9-2.4 ppb) than the RO_2 concentrations (0.1-2.2 ppt) (Table 1), which hints that the formation of closed-shell C_x products is limited by the RO_2 availability. Indeed, good correlations between closed-shell C_x products and RO_2 are observed (Figure 3). The slopes are generally lower for double-ring precursors than for monocyclic precursors, indicating a steric hindrance of double rings on the C_x product formation.

For a given precursor of C_xH_y, further auto-oxidation of BPRs ($C_xH_{y+1}O_5$) may lead to the formation of C_x products with hydrogen numbers of y or y+2, whereas multi-generation OH reactions (i.e., a second or third OH attack) would lead to the formation of C_x products with hydrogen numbers of y-2 (H abstraction) or > y+2 (OH addition) (Garmash et al., 2020; Cheng et al., 2021b). Figure 4 shows the signal fractions of closed-shell C_x products that have different hydrogen numbers at

https://doi.org/10.5194/egusphere-2023-1215
Preprint. Discussion started: 10 July 2023

different OH exposure. The signal fractions of products with y-2 hydrogen numbers increase with increasing OH exposure, suggesting that more H abstraction may have occurred at higher OH exposure. Consistently, the signal fractions of C_x products with > y+2 hydrogen numbers decrease as the OH exposure increases, suggesting less OH addition at higher OH exposure. H abstraction has been found to be involved in the formation of the majority of monoterpene OOMs (Shen et al., 2022). Moreover, the signal fractions of products with y-2 and > y+2 hydrogen numbers are relatively higher in naphthalene- and 1-methylnaphthalene-derived OOMs than in other types of OOMs, highlighting the importance of multi-generation OH oxidation for double-ring aromatic precursors. Additionally, for naphthalene and 1-methylnaphthalene, the products with y+4 or y+6 hydrogen numbers have high signals, whereas for monocyclic aromatic OOMs, the products with y+4 hydrogen numbers are the main > y+2 products (Tables S1-S6 and Figure S3). The presence of abundant C_x products with hydrogen numbers of y+6 from double-ring precursors suggests a significant occurrence of third OH addition on early-generation products that still possess a high degree of unsaturation.

The concentrations of C_{2x} products are several times lower than those of C_x products (Figure S4). They correlate well with the square of the RO_2 concentrations (Figure 5). The slopes are lower for naphthalene and 1-methylnaphthalene than for monocyclic precursors, suggesting again significant steric effects on the formation of C_{2x} products (Tomaz et al., 2021). Table 2 lists the resolved rate constants for benzene- and naphthalene-derived dimeric products with reasonable fittings (r > 0.5). Our estimated rate coefficients for C_{2x} products from the self- and cross-reactions of RO_2 radicals span a range of one order of magnitude (i.e., 0.9-8.5×10^{-10} cm^3 $molecule^{-1}$ s^{-1}). The rates are similar to those reported for α-pinene + OH/O_3 and 1,3,5-trimethylbenzene + O_3/OH (i.e., 0.1-8.7×10^{-10} cm^3 $molecule^{-1}$ s^{-1}) (Berndt et al., 2018a; Berndt et al., 2018b; Molteni et al., 2019). The rate constant for benzene-derived dimer $C_{12}H_{14}O_{15}$ from $C_6H_7O_8$ + $C_6H_7O_9$ (7.0×10^{-10} cm^3 $molecules^{-1}$ s^{-1}) is nearly 8 times greater than that for naphthalene-derived dimer $C_{20}H_{18}O_{14}$ from $C_{10}H_9O_8$ + $C_{10}H_9O_8$ (0.9×10^{-10} cm^3 $molecules^{-1}$ s^{-1}), suggesting that the apparent accretion reaction rate constants are sensitive to precursor structures and RO_2 functional groups. These RO_2 radicals could be formed from BPRs ($C_xH_{y+1}O_5$), thus the lower values for $C_{20}H_{18}O_{14}$ can be related with the steric influence of double rings.

3.3 OOM Contribution to SOA

Figure 6 shows the average elemental ratios of SOA and detected gaseous OOMs as well as the estimated contributions of the detected OOMs to the SOA mass for the experiments having AMS and SMPS particle measurements. For the three types of aromatic SOA, most of the O:C ratios are much greater while the H:C ratios are lower compared to the reported values in previous chamber studies (Nakao et al., 2013; Chhabra et al., 2010; Kautzman et al., 2010) (Figure 6a). This is because higher OH exposure levels in the OFR lead to the formation of SOA with higher average carbon oxidation state (Kroll et al., 2011). Our results agree with the reported O:C ratios in another OFR study (i.e., 0.86-1.40 for toluene SOA and 0.48-1.59 for naphthalene SOA) (Lambe et al., 2011). Similar to the elemental ratios of SOA, the detected OOMs produced from naphthalene have lower O:C and lower H:C ratios than those from benzene and toluene (Figure 6b). When the OH exposure

https://doi.org/10.5194/egusphere-2023-1215
Preprint. Discussion started: 10 July 2023

increases, the average O:C ratios of the detected OOMs increase and the H:C ratios decrease (Figure S5). The increase of O:C ratios of OOMs is more significant for the oxidation of naphthalene, whereas the decrease of H:C ratios of OOMs is more evident for the oxidation of benzene and toluene. All these trends are consistent with those observed for SOA, though the much broader ranges of O:C and H:C for each type of SOA than those for detected OOMs highlight the important contributions of undetected products to SOA.

The estimated contributions of these OOMs to the SOA mass are 3.1-5.4%, 6.5-10.8%, and 7.4-10.1% for the oxidation of benzene, toluene, and naphthalene, respectively (Figure 6c). As shown in Figure S6, most of the identified OOMs are in the SVOC and LVOC ranges, and the volatility distribution of OOMs from naphthalene appears to be lower than those of benzene and toluene. A recent field study in the urbanized regions of China suggested that the detected aromatic OOMs are the dominant source of the SOA mass (~50-70%) (Nie et al., 2022). We only found 3-11% of mass contributions of NO_3^--TOF-CIMS detectable OOMs to the aromatic SOA. Large uncertainties remain in the estimation, and the OFR experiments may not mimic fully the ambient conditions. The mixed precursors in real urban air may affect the RO_2 chemistry and the product distributions (Chen et al., 2022).

Notably, the O:C ratios of naphthalene-derived OOMs are much lower than those of benzene-derived OOMs, but the naphthalene-derived OOMs contain more low-volatility fractions than those of benzene-derived OOMs as shown in the volatility distribution (Figure S6). The contributions of the detected OOMs to the SOA mass are about 2 times greater than those for benzene, which is consistent with the volatility distributions. Both observations are related to the intrinsically large carbon number in naphthalene than that in benzene. Field measurements in urban Shanghai suggest that heavy aromatic VOCs are important SOA precursors (Tian et al., 2022). The results herein provide laboratory evidence that heavy (e.g., double-ring) aromatic VOCs might be more important than light (i.e., monocyclic) aromatic ones in initial particle growth during SOA formation.

4 Conclusions

The formation of OOMs from the photooxidation of benzene, toluene, m-xylene, 1,3,5-trimethylbenzene, naphthalene, and 1-methylnaphthalene was investigated under low-NO_x conditions with a wide range of OH exposure. The detected OOM formulae show diverse oxygen and hydrogen numbers that need both of multi-step auto-oxidation and multi-generation OH oxidation to explain, highlighting similar reaction rates of the two mechanisms under atmospheric relevant VOC concentrations. Multi-generation OH oxidation appears to be more prominent at higher OH exposure for the oxidation of double-ring precursors than for the oxidation of single-ring aromatic precursors. The product distributions also demonstrate significant steric effects of the methyl substitution and the double-ring structure on the OOM formation. We show that (1) the formation of fragmented products, especially unsaturated small oxygenates, are less efficient for precursors with more methyl groups, and (2) the steric effects of double rings affect the formation of both of monomeric and dimeric products.

https://doi.org/10.5194/egusphere-2023-1215
Preprint. Discussion started: 10 July 2023

More studies are needed for developing quantitative understanding to improve the CTM representation. Finally, we found more OOMs produced by the oxidation of double-ring precursors in the lower volatility range than those formed from the oxidation of traditional monocyclic precursors, highlighting the importance of heavy aromatics to SOA formation. The detectable OOMs by the NO_3^--TOF-CIMS are usually highly oxygenated products and explain only 3-11% of the SOA mas. More of the SOA mass are perhaps contributed by less oxygenated products that require other types of chemical ionization technique to explore.

Data availability. Data presented in this manuscript are available upon request to the corresponding author.

Author contributions. QC and YJL designed the study. XC, YZ, and KL conducted the experiments. XC performed the data analysis with the help of all authors. XC, QC, and YJL wrote the manuscript with inputs from all other authors.

Competing interests. At least one of the (co-)authors is a member of the editorial board of Atmospheric Chemistry and Physics. The peer-review process was guided by an independent editor, and the authors also have no other competing interests to declare.

Financial support. This work is supported by the National Natural Science Foundation of China (41875165, 41961134034) and the 111 Project of Urban Air Pollution and Health Effects (B20009). YJL acknowledges funding support from the Science and Technology Development Fund, Macao SAR (File no. 0023/2021/A1) and a multiyear research grant (No. MYRG2022-00027-FST) from the University of Macau. The authors gratefully acknowledge Andrew Lambe, and Penglin Ye for instrument support and helpful discussion.

References

Aiken, A. C., Decarlo, P. F., Kroll, J. H., Worsnop, D. R., Huffman, J. A., Docherty, K. S., Ulbrich, I. M., Mohr, C., Kimmel, J. R., Sueper, D., Sun, Y., Zhang, Q., Trimborn, A., Northway, M., Ziemann, P. J., Canagaratna, M. R., Onasch, T. B., Alfarra, M. R., Prevot, A. S. H., Dommen, J., Duplissy, J., Metzger, A., Baltensperger, U., and Jimenez, J. L.: O/C and OM/OC ratios of primary, secondary, and ambient organic aerosols with high-resolution time-of-flight aerosol mass spectrometry, Environ. Sci. Technol., 42, 4478-4485, https://doi.org/10.1021/es703009q, 2008.

Berndt, T., Mentler, B., Scholz, W., Fischer, L., Herrmann, H., Kulmala, M., and Hansel, A.: Accretion product formation from ozonolysis and OH radical reaction of α-Pinene: mechanistic insight and the influence of isoprene and ethylene, Environ. Sci. Technol., 52, 11069-11077, https://doi.org/10.1021/acs.est.8b02210, 2018a.

https://doi.org/10.5194/egusphere-2023-1215
Preprint. Discussion started: 10 July 2023

Berndt, T., Scholz, W., Mentler, B., Fischer, L., Herrmann, H., Kulmala, M., and Hansel, A.: Accretion product formation from self- and cross-reactions of RO2 radicals in the atmosphere, Angew. Chemie, 57, 3820-3824, https://doi.org/10.1002/anie.201710989, 2018b.

Bianchi, F., Kurten, T., Riva, M., Mohr, C., Rissanen, M. P., Roldin, P., Berndt, T., Crounse, J. D., Wennberg, P. O., Mentel, T. F., Wildt, J., Junninen, H., Jokinen, T., Kulmala, M., Worsnop, D. R., Thornton, J. A., Donahue, N., Kjaergaard, H. G., and Ehn, M.: Highly oxygenated organic molecules (HOM) from gas-phase autoxidation involving peroxy radicals: a key contributor to atmospheric aerosol, Chem. Rev., 119, 3472-3509, https://doi.org/10.1021/acs.chemrev.8b00395, 2019.

Birdsall, A. W., Andreoni, J. F., and Elrod, M. J.: Investigation of the role of bicyclic peroxy radicals in the oxidation mechanism of toluene, J. Phys. Chem. A, 114, 10655-10663, https://doi.org/10.1021/jp105467e, 2010.

Chan, A. W. H., Kautzman, K. E., Chhabra, P. S., Surratt, J. D., Chan, M. N., Crounse, J. D., Kuerten, A., Wennberg, P. O., Flagan, R. C., and Seinfeld, J. H.: Secondary organic aerosol formation from photooxidation of naphthalene and alkylnaphthalenes: implications for oxidation of intermediate volatility organic compounds (IVOCs), Atmos. Chem. Phys., 9, 3049-3060, https://doi.org/10.5194/acp-9-3049-2009, 2009.

Chen, Q., Liu, Y., Donahue, N. M., Shilling, J. E., and Martin, S. T.: Particle-phase chemistry of secondary organic material: modeled compared to measured O:C and H:C elemental ratios provide constraints, Environ. Sci. Technol., 45, 4763-4770, https://doi.org/10.1021/es104398s, 2011.

Chen, T., Zhang, P., Chu, B., Ma, Q., Ge, Y., Liu, J., and He, H.: Secondary organic aerosol formation from mixed volatile organic compounds: Effect of RO2 chemistry and precursor concentration, npj Climate and Atmospheric Science, 5, 95, https://doi.org/10.1038/s41612-022-00321-y, 2022.

Cheng, X., Chen, Q., Li, Y., Huang, G., Liu, Y., Lu, S., Zheng, Y., Qiu, W., Lu, K., Qiu, X., Bianchi, F., Yan, C., Yuan, B., Shao, M., Wang, Z., Canagaratna, M. R., Zhu, T., Wu, Y., and Zeng, L.: Secondary production of gaseous nitrated phenols in polluted urban environments, Environ. Sci. Technol., 55, 4410-4419, https://doi.org/10.1021/acs.est.0c07988, 2021a.

Cheng, X., Chen, Q., Li, Y., Zheng, Y., Liao, K., and Huang, G.: Highly oxygenated organic molecules produced by the oxidation of benzene and toluene in a wide range of OH exposure and NOx conditions, Atmos. Chem. Phys., 21, 12005-12019, https://doi.org/10.5194/acp-21-12005-2021, 2021b.

Chhabra, P. S., Flagan, R. C., and Seinfeld, J. H.: Elemental analysis of chamber organic aerosol using an aerodyne high-resolution aerosol mass spectrometer, Atmos. Chem. Phys., 10, 4111-4131, https://doi.org/10.5194/acp-10-4111-2010, 2010.

Chhabra, P. S., Ng, N. L., Canagaratna, M. R., Corrigan, A. L., Russell, L. M., Worsnop, D. R., Flagan, R. C., and Seinfeld, J. H.: Elemental composition and oxidation of chamber organic aerosol, Atmos. Chem. Phys., 11, 8827-8845, https://doi.org/10.5194/acp-11-8827-2011, 2011.

Donahue, N. M., Robinson, A. L., Stanier, C. O., and Pandis, S. N.: Coupled partitioning, dilution, and chemical aging of semivolatile organics, Environ. Sci. Technol., 40, 2635-2643, https://doi.org/10.1021/es052297c, 2006.

Garmash, O., Rissanen, M. P., Pullinen, I., Schmitt, S., Kausiala, O., Tillmann, R., Zhao, D., Percival, C., Bannan, T. J., Priestley, M., Hallquist, Å. M., Kleist, E., Kiendler-Scharr, A., Hallquist, M., Berndt, T., McFiggans, G., Wildt, J., Mentel, T.

https://doi.org/10.5194/egusphere-2023-1215
Preprint. Discussion started: 10 July 2023

F., and Ehn, M.: Multi-generation OH oxidation as a source for highly oxygenated organic molecules from aromatics, Atmos. Chem. Phys., 20, 515-537, https://doi.org/10.5194/acp-20-515-2020, 2020.

Henze, D. K., Seinfeld, J. H., Ng, N. L., Kroll, J. H., Fu, T. M., Jacob, D. J., and Heald, C. L.: Global modeling of secondary organic aerosol formation from aromatic hydrocarbons: high- vs. low-yield pathways, Atmos. Chem. Phys., 8, 2405-2420, https://doi.org/10.5194/acp-8-2405-2008, 2008.

Huang, G., Liu, Y., Shao, M., Li, Y., Chen, Q., Zheng, Y., Wu, Z., Liu, Y., Wu, Y., Hu, M., Li, X., Lu, S., Wang, C., Liu, J., Zheng, M., and Zhu, T.: Potentially important contribution of gas-phase oxidation of naphthalene and methylnaphthalene to secondary organic aerosol during haze events in Beijing, Environ. Sci. Technol., 53, 1235-1244, https://doi.org/10.1021/acs.est.8b04523, 2019.

Kautzman, K. E., Surratt, J. D., Chan, M. N., Chan, A. W. H., Hersey, S. P., Chhabra, P. S., Dalleska, N. F., Wennberg, P. O., Flagan, R. C., and Seinfeld, J. H.: Chemical composition of gas- and aerosol-phase products from the photooxidation of naphthalene, J. Phys. Chem. A, 114, 913-934, https://doi.org/10.1021/jp908530s, 2010.

Kroll, J. H., Donahue, N. M., Jimenez, J. L., Kessler, S. H., Canagaratna, M. R., Wilson, K. R., Altieri, K. E., Mazzoleni, L. R., Wozniak, A. S., Bluhm, H., Mysak, E. R., Smith, J. D., Kolb, C. E., and Worsnop, D. R.: Carbon oxidation state as a metric for describing the chemistry of atmospheric organic aerosol, Nature Chem., 3, 133, https://doi.org/10.1038/nchem.948 https://www.nature.com/articles/nchem.948#supplementary-information, 2011.

Lambe, A., Massoli, P., Zhang, X., Canagaratna, M., Nowak, J., Daube, C., Yan, C., Nie, W., Onasch, T., Jayne, J., Kolb, C., Davidovits, P., Worsnop, D., and Brune, W.: Controlled nitric oxide production via O(1-D) + N2O reactions for use in oxidation flow reactor studies, Atmos. Meas. Tech., 10, 2283-2298, https://doi.org/10.5194/amt-10-2283-2017, 2017.

Lambe, A. T., Onasch, T. B., Massoli, P., Croasdale, D. R., Wright, J. P., Ahern, A. T., Williams, L. R., Worsnop, D. R., Brune, W. H., and Davidovits, P.: Laboratory studies of the chemical composition and cloud condensation nuclei (CCN) activity of secondary organic aerosol (SOA) and oxidized primary organic aerosol (OPOA), Atmos. Chem. Phys., 11, 8913-8928, https://doi.org/10.5194/acp-11-8913-2011, 2011.

Li, L., Tang, P., Nakao, S., Chen, C. L., and Cocker, D. R., III: Role of methyl group number on SOA formation from monocyclic aromatic hydrocarbons photooxidation under low-NOx conditions, Atmos. Chem. Phys., 16, 2255-2272, https://doi.org/10.5194/acp-16-2255-2016, 2016a.

Li, L. J., Tang, P., Nakao, S., and Cocker, D. R.: Impact of molecular structure on secondary organic aerosol formation from aromatic hydrocarbon photooxidation under low-NOx conditions, Atmos. Chem. Phys., 16, 10793-10808, https://doi.org/10.5194/acp-16-10793-2016, 2016b.

Li, Y., and Wang, L.: The atmospheric oxidation mechanism of 1,2,4-trimethylbenzene initiated by OH radicals, Phys. Chem. Chem. Phys., 16, 17908-17917, https://doi.org/10.1039/c4cp02027h, 2014.

Mehra, A., Wang, Y., Krechmer, J. E., Lambe, A., Majluf, F., Morris, M. A., Priestley, M., Bannan, T. J., Bryant, D. J., Pereira, K. L., Hamilton, J. F., Rickard, A. R., Newland, M. J., Stark, H., Croteau, P., Jayne, J. T., Worsnop, D. R.,

https://doi.org/10.5194/egusphere-2023-1215
Preprint. Discussion started: 10 July 2023

Canagaratna, M. R., Wang, L., and Coe, H.: Evaluation of the chemical composition of gas- and particle-phase products of aromatic oxidation, Atmos. Chem. Phys., 20, 9783-9803, https://doi.org/10.5194/acp-20-9783-2020, 2020.

Mohr, C., Thornton, J. A., Heitto, A., Lopez-Hilfiker, F. D., Lutz, A., Riipinen, I., Hong, J., Donahue, N. M., Hallquist, M., Petaja, T., Kulmala, M., and Yli-Juuti, T.: Molecular identification of organic vapors driving atmospheric nanoparticle growth, Nat. Commun., 10, https://doi.org/10.1038/s41467-019-12473-2, 2019.

Molteni, U., Bianchi, F., Klein, F., El Haddad, I., Frege, C., Rossi, M. J., Dommen, J., and Baltensperger, U.: Formation of highly oxygenated organic molecules from aromatic compounds, Atmos. Chem. Phys., 18, 1909-1921, https://doi.org/10.5194/acp-18-1909-2018, 2018.

Molteni, U., Simon, M., Heinritzi, M., Hoyle, C. R., Bernhammer, A.-K., Bianchi, F., Breitenlechner, M., Brilke, S., Dias, A., Duplissy, J., Frege, C., Gordon, H., Heyn, C., Jokinen, T., Kuerten, A., Lehtipalo, K., Makhmutov, V., Petaja, T., Pieber, S. M., Praplan, A. P., Schobesberger, S., Steiner, G., Stozhkov, Y., Tome, A., Trostl, J., Wagner, A. C., Wagner, R., Williamson, C., Yan, C., Baltensperger, U., Curtius, J., Donahue, N. M., Hansel, A., Kirkby, J., Kulmala, M., Worsnop, D. R., and Dommen, J.: Formation of highly oxygenated organic molecules from α-pinene ozonolysis: chemical characteristics, mechanism, and kinetic model development, ACS Earth Space Chem., 3, 873-883, https://doi.org/10.1021/acsearthspacechem.9b00035, 2019.

Nakao, S., Tang, P., Tang, X., Clark, C. H., Qi, L., Seo, E., Asa-Awuku, A., and Cocker, D., III: Density and elemental ratios of secondary organic aerosol: application of a density prediction method, Atmos. Environ., 68, 273-277, https://doi.org/10.1016/j.atmosenv.2012.11.006, 2013.

Ng, N. L., Kroll, J. H., Chan, A. W. H., Chhabra, P. S., Flagan, R. C., and Seinfeld, J. H.: Secondary organic aerosol formation from m-xylene, toluene, and benzene, Atmos. Chem. Phys., 7, 3909-3922, https://doi.org/10.5194/acp-7-3909-2007, 2007.

Nie, W., Yan, C., Huang, D. D., Wang, Z., Liu, Y. L., Qiao, X. H., Guo, Y. S., Tian, L. H., Zheng, P. G., Xu, Z. N., Li, Y. Y., Xu, Z., Qi, X. M., Sun, P., Wang, J. P., Zheng, F. X., Li, X. X., Yin, R. J., Dallenbach, K. R., Bianchi, F., Petaja, T., Zhang, Y. J., Wang, M. Y., Schervish, M., Wang, S. N., Qiao, L. P., Wang, Q., Zhou, M., Wang, H. L., Yu, C. A., Yao, D. W., Guo, H., Ye, P. L., Lee, S. C., Li, Y. J., Liu, Y. C., Chi, X. G., Kerminen, V. M., Ehn, M., Donahue, N. M., Wang, T., Huang, C., Kulmala, M., Worsnop, D., Jiang, J. K., and Ding, A. J.: Secondary organic aerosol formed by condensing anthropogenic vapours over China's megacities, Nat. Geosci., 15, 255-261, https://doi.org/10.1038/s41561-022-00922-5, 2022.

Orlando, J. J., Tyndall, G. S., and Wallington, T. J.: The atmospheric chemistry of alkoxy radicals, Chem. Rev., 103, 4657-4690, https://doi.org/10.1021/cr020527p, 2003.

Pankow, J. F.: An absorption model of gas/particle partitioning of organic compounds in the atmosphere, Atmos. Environ., 28, 185-188, https://doi.org/10.1016/1352-2310(94)90093-0, 1994.

Peng, Z., Day, D. A., Ortega, A. M., Palm, B. B., Hu, W. W., Stark, H., Li, R., Tsigaridis, K., Brune, W. H., and Jimenez, J. L.: Non-OH chemistry in oxidation flow reactors for the study of atmospheric chemistry systematically examined by modeling, Atmos. Chem. Phys., 16, 4283-4305, https://doi.org/10.5194/acp-16-4283-2016, 2016.

https://doi.org/10.5194/egusphere-2023-1215
Preprint. Discussion started: 10 July 2023

Peng, Z., Palm, B. B., Day, D. A., Talukdar, R. K., Hu, W. W., Lambe, A. T., Brune, W. H., and Jimenez, J. L.: Model evaluation of new techniques for maintaining high-NO conditions in oxidation flow reactors for the study of OH-initiated atmospheric chemistry, ACS Earth Space Chem., 2, 72-86, https://doi.org/10.1021/acsearthspacechem.7b00070, 2018.

Pye, H. O. T., and Pouliot, G. A.: Modeling the role of alkanes, polycyclic aromatic hydrocarbons, and their oligomers in secondary organic aerosol formation, Environ. Sci. Technol., 46, 6041-6047, https://doi.org/10.1021/es300409w, 2012.

Schervish, M., and Donahue, N. M.: Peroxy radical chemistry and the volatility basis set, Atmos. Chem. Phys., 20, 1183-1199, https://doi.org/10.5194/acp-20-1183-2020, 2020.

Schwantes, R. H., Schilling, K. A., McVay, R. C., Lignell, H., Coggon, M. M., Zhang, X., Wennberg, P. O., and Seinfeld, J. H.: Formation of highly oxygenated low-volatility products from cresol oxidation, Atmos. Chem. Phys., 17, 3453-3474, https://doi.org/10.5194/acp-17-3453-2017, 2017.

Shen, H., Vereecken, L., Kang, S., Pullinen, I., Fuchs, H., Zhao, D., and Mentel, T. F.: Unexpected significance of a minor reaction pathway in daytime formation of biogenic highly oxygenated organic compounds, Sci. Adv., 8, eabp8702, https://doi.org/10.1126/sciadv.abp8702, 2022.

Tian, L., Huang, D. D., Wang, Q., Zhu, S., Wang, Q., Yan, C., Nie, W., Wang, Z., Qiao, L., Liu, Y., Qiao, X., Guo, Y., Zheng, P., Jing, S. a., Lou, S., Wang, H., Yu, J. Z., Huang, C., and Li, Y. J.: Underestimated contribution of heavy aromatics to secondary organic aerosol revealed by comparative assessments using new and traditional methods, ACS Earth Space Chem., https://doi.org/10.1021/acsearthspacechem.2c00252, 2022.

Tomaz, S., Wang, D., Zabalegui, N., Li, D., Lamkaddam, H., Bachmeier, F., Vogel, A., Monge, M. E., Perrier, S., Baltensperger, U., George, C., Rissanen, M., Ehn, M., El Haddad, I., and Riva, M.: Structures and reactivity of peroxy radicals and dimeric products revealed by online tandem mass spectrometry, Nat. Commun., 12, 300, https://doi.org/10.1038/s41467-020-20532-2, 2021.

Tröstl, J., Chuang, W. K., Gordon, H., Heinritzi, M., Yan, C., Molteni, U., Ahlm, L., Frege, C., Bianchi, F., Wagner, R., Simon, M., Lehtipalo, K., Williamson, C., Craven, J. S., Duplissy, J., Adamov, A., Almeida, J., Bernhammer, A.-K., Breitenlechner, M., Brilke, S., Dias, A., Ehrhart, S., Flagan, R. C., Franchin, A., Fuchs, C., Guida, R., Gysel, M., Hansel, A., Hoyle, C. R., Jokinen, T., Junninen, H., Kangasluoma, J., Keskinen, H., Kim, J., Krapf, M., Kürten, A., Laaksonen, A., Lawler, M., Leiminger, M., Mathot, S., Möhler, O., Nieminen, T., Onnela, A., Petäjä, T., Piel, F. M., Miettinen, P., Rissanen, M. P., Rondo, L., Sarnela, N., Schobesberger, S., Sengupta, K., Sipilä, M., Smith, J. N., Steiner, G., Tomè, A., Virtanen, A., Wagner, A. C., Weingartner, E., Wimmer, D., Winkler, P. M., Ye, P., Carslaw, K. S., Curtius, J., Dommen, J., Kirkby, J., Kulmala, M., Riipinen, I., Worsnop, D. R., Donahue, N. M., and Baltensperger, U.: The role of low-volatility organic compounds in initial particle growth in the atmosphere, Nature, 533, 527-531, https://doi.org/10.1038/nature18271, 2016.

Tsigaridis, K., Daskalakis, N., Kanakidou, M., Adams, P. J., Artaxo, P., Bahadur, R., Balkanski, Y., Bauer, S. E., Bellouin, N., Benedetti, A., Bergman, T., Berntsen, T. K., Beukes, J. P., Bian, H., Carslaw, K. S., Chin, M., Curci, G., Diehl, T., Easter, R. C., Ghan, S. J., Gong, S. L., Hodzic, A., Hoyle, C. R., Iversen, T., Jathar, S., Jimenez, J. L., Kaiser, J. W., Kirkevag, A., Koch, D., Kokkola, H., Lee, Y. H., Lin, G., Liu, X., Luo, G., Ma, X., Mann, G. W., Mihalopoulos, N., Morcrette, J. J.,

https://doi.org/10.5194/egusphere-2023-1215
Preprint. Discussion started: 10 July 2023

Muller, J. F., Myhre, G., Myriokefalitakis, S., Ng, N. L., O'Donnell, D., Penner, J. E., Pozzoli, L., Pringle, K. J., Russell, L. M., Schulz, M., Sciare, J., Seland, O., Shindell, D. T., Sillman, S., Skeie, R. B., Spracklen, D., Stavrakou, T., Steenrod, S. D., Takemura, T., Tiitta, P., Tilmes, S., Tost, H., van Noije, T., van Zyl, P. G., von Salzen, K., Yu, F., Wang, Z., Wang, Z., Zaveri, R. A., Zhang, H., Zhang, K., Zhang, Q., and Zhang, X.: The AeroCom evaluation and intercomparison of organic aerosol in global models, Atmos. Chem. Phys., 14, 10845-10895, https://doi.org/10.5194/acp-14-10845-2014, 2014.

Wang, S., Wu, R., Berndt, T., Ehn, M., and Wang, L.: Formation of highly oxidized radicals and multifunctional products from the atmospheric oxidation of alkylbenzenes, Environ. Sci. Technol., 51, 8442-8449, https://doi.org/10.1021/acs.est.7b02374, 2017.

Wang, Y., Mehra, A., Krechmer, J. E., Yang, G., Hu, X., Lu, Y., Lambe, A., Canagaratna, M., Chen, J., Worsnop, D., Coe, H., and Wang, L.: Oxygenated products formed from OH-initiated reactions of trimethylbenzene: autoxidation and accretion, Atmos. Chem. Phys., 20, 9563-9579, https://doi.org/10.5194/acp-20-9563-2020, 2020.

Zaytsev, A., Koss, A. R., Breitenlechner, M., Krechmer, J. E., Nihill, K. J., Lim, C. Y., Rowe, J. C., Cox, J. L., Moss, J., Roscioli, J. R., Canagaratna, M. R., Worsnop, D. R., Kroll, J. H., and Keutsch, F. N.: Mechanistic study of the formation of ring-retaining and ring-opening products from the oxidation of aromatic compounds under urban atmospheric conditions, Atmos. Chem. Phys., 19, 15117-15129, https://doi.org/10.5194/acp-19-15117-2019, 2019.

Zhao, Y., Thornton, J. A., and Pye, H. O. T.: Quantitative constraints on autoxidation and dimer formation from direct probing of monoterpene-derived peroxy radical chemistry, Proc. Natl. Acad. Sci. U. S. A., 115, 12142-12147, https://doi.org/10.1073/pnas.1812147115, 2018.

Zheng, Y., Cheng, X., Liao, K. R., Li, Y. W., Li, Y. J., Hu, W. W., Liu, Y., Zhu, T., Chen, S. Y., Zeng, L. M., Worsnop, D., Chen, Q., and Huang, R. J.: Characterization of anthropogenic organic aerosols by TOF-ACSM with the new capture vaporizer, Atmos. Meas. Tech., 13, 2457-2472, https://doi.org/10.5194/amt-13-2457-2020, 2020.

Ziemann, P. J., and Atkinson, R.: Kinetics, products, and mechanisms of secondary organic aerosol formation, Chem. Soc. Rev., 41, 6582-6605, https://doi.org/10.1039/C2CS35122F, 2012.

https://doi.org/10.5194/egusphere-2023-1215
Preprint. Discussion started: 10 July 2023

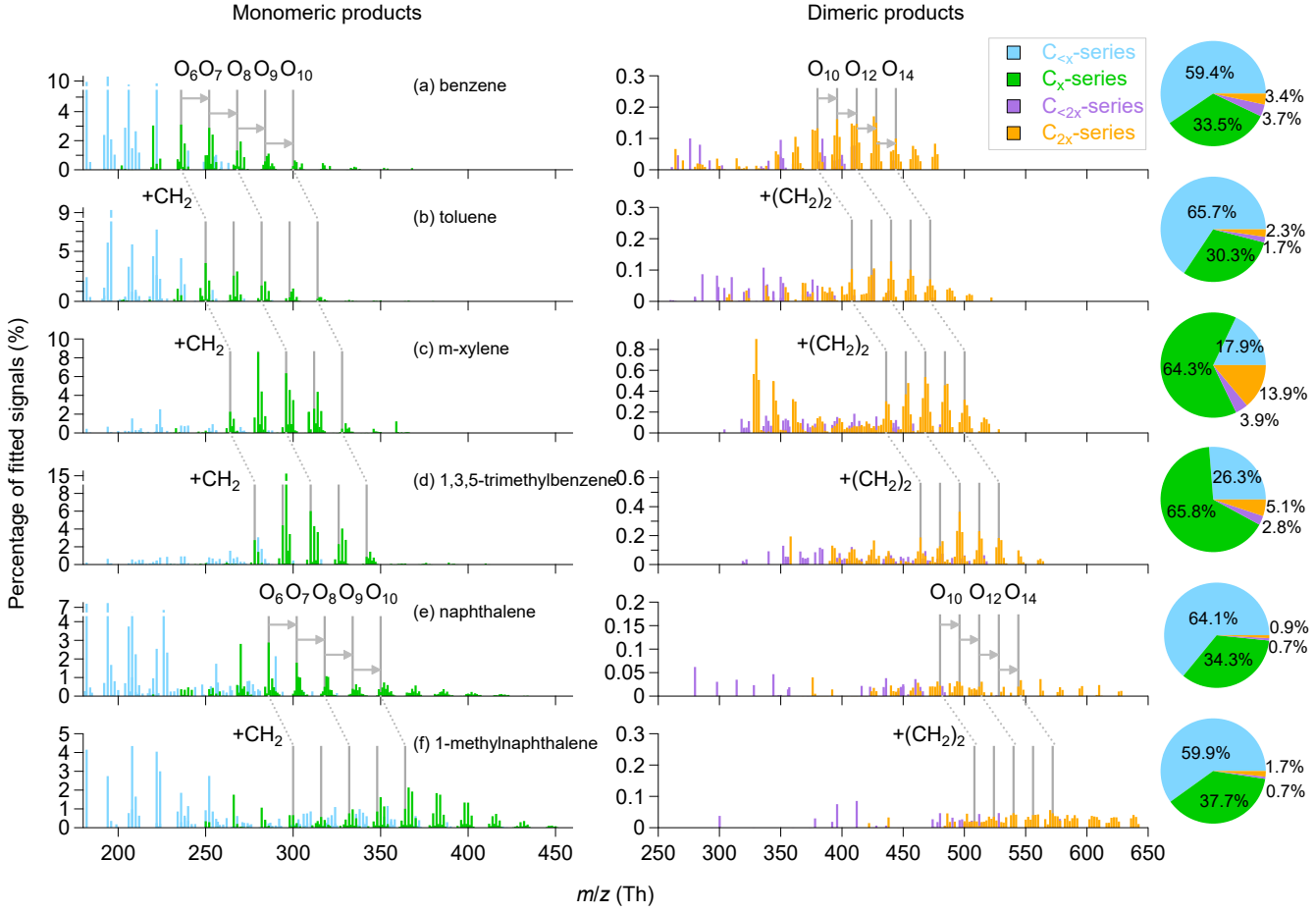

Figure 1. Mass spectra and fractions of different categories of gaseous OOMs observed in the oxidation of **(a)** benzene, **(b)** toluene, **(c)** m-xylene, **(d)** 1,3,5-trimethylbenzene, **(e)** naphthalene and **(f)** 1-methylnaphthalene, corresponding to experiments No. 2, 7, 12, 16, 22 and 26 in Table 1, respectively.

https://doi.org/10.5194/egusphere-2023-1215
Preprint. Discussion started: 10 July 2023

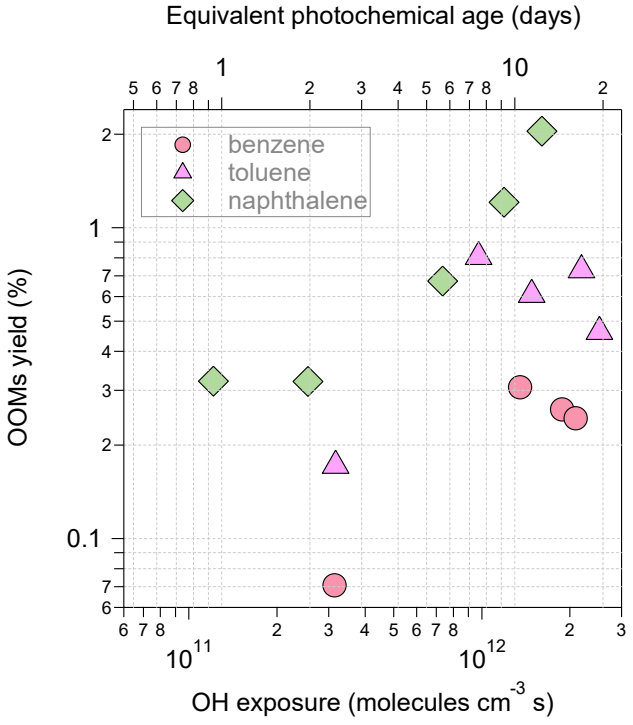

Figure 2. Yields of OOMs produced from photooxidation of benzene, toluene, and naphthalene in OFR as a function of OH exposure. Equivalent photochemical ages are referred to a mean OH concentration of 1.5×10^6 molecules cm^{-3}.

https://doi.org/10.5194/egusphere-2023-1215
Preprint. Discussion started: 10 July 2023

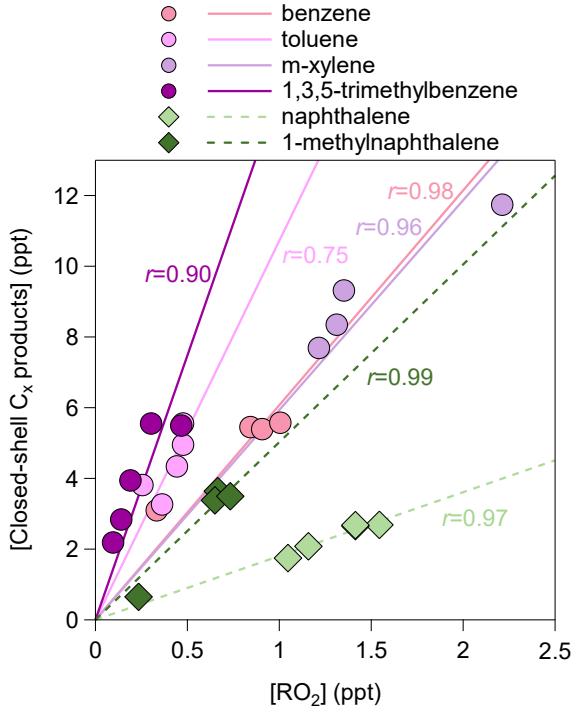

485

Figure 3. Scatter plot of the concentrations of closed-shell C_x products and those of open-shell C_x products (RO_2) for the 27 experiments listed in Table 1. The *r* values represent the Pearson correlation coefficients.

https://doi.org/10.5194/egusphere-2023-1215
Preprint. Discussion started: 10 July 2023

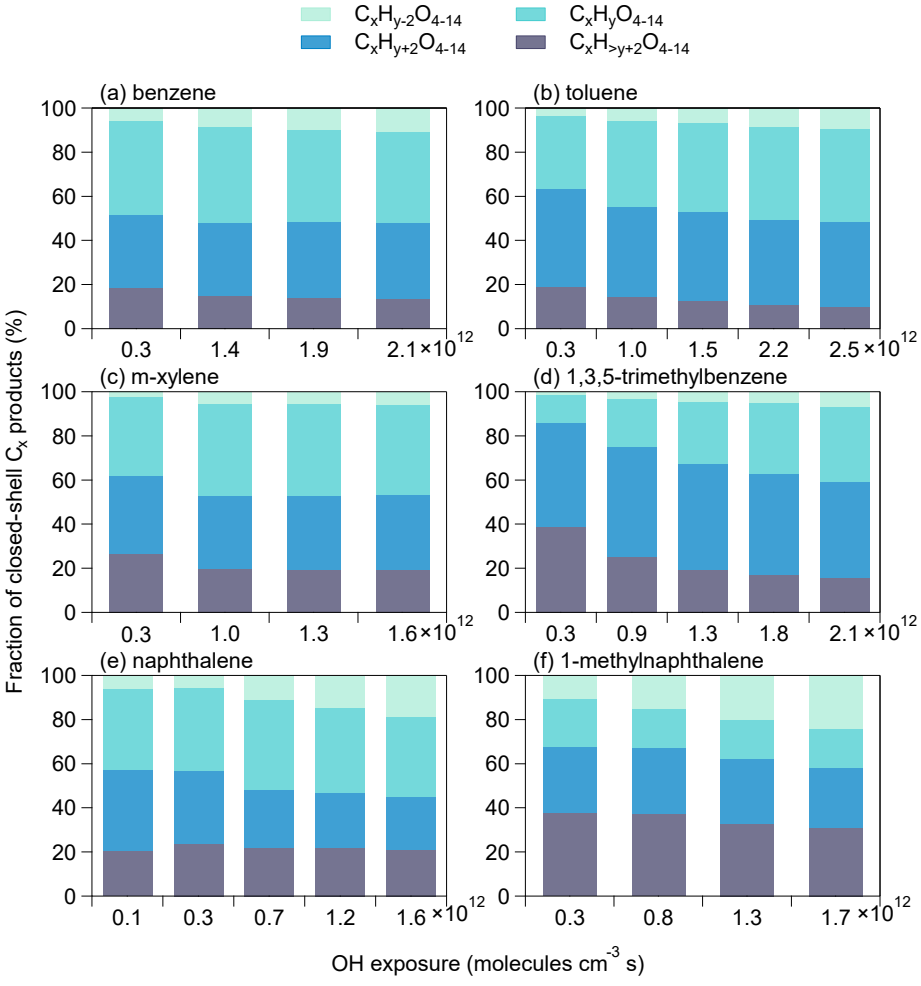

Figure 4. Fractions of different series of closed-shell C_x products formed from the oxidation of **(a)** benzene, **(b)** toluene, **(c)** m-xylene, **(d)** 1,3,5-trimethylbenzene, **(e)** naphthalene and **(f)** 1-methylnaphthalene at different OH exposure. *x* and *y* represent the numbers of carbon and hydrogen atoms of the aromatic precursor (C_xH_y).

https://doi.org/10.5194/egusphere-2023-1215
Preprint. Discussion started: 10 July 2023

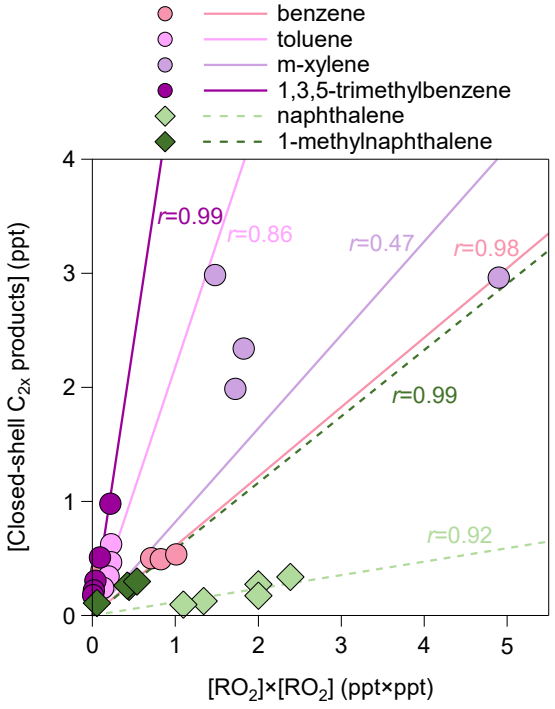

Figure 5. Scatter plot of the concentrations of closed-shell C_{2x} products and those of $RO_2 \times RO_2$ for the 27 experiments listed in Table 1. The *r* values represent the Pearson correlation coefficients.

https://doi.org/10.5194/egusphere-2023-1215
Preprint. Discussion started: 10 July 2023

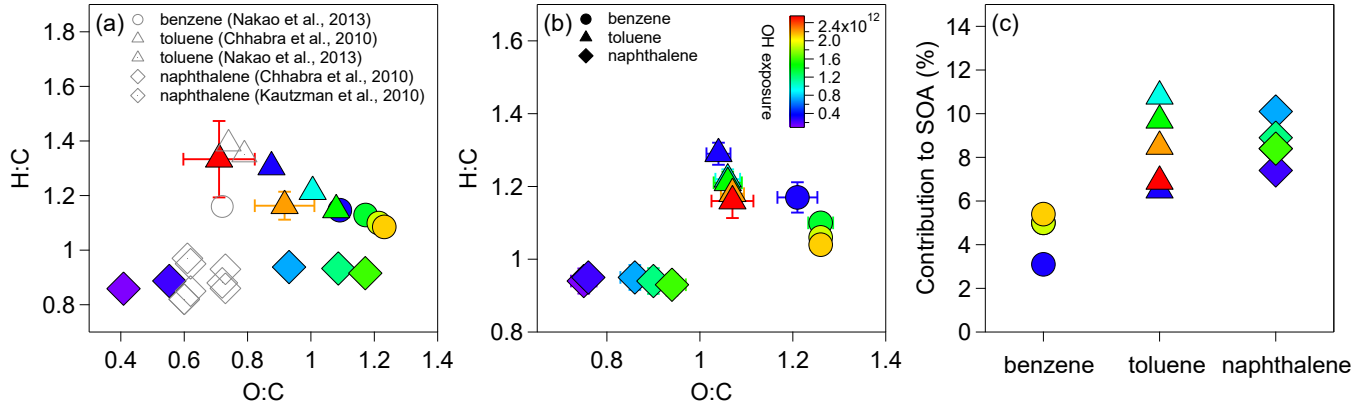

Figure 6. (a) H:C and O:C ratios of the resulted SOA for the oxidation of benzene, toluene and naphthalene. **(b)** H:C and O:C ratios of gaseous OOMs detected in these experiments. **(c)** Estimated contributions of the detected OOMs to the SOA mass.

https://doi.org/10.5194/egusphere-2023-1215
Preprint. Discussion started: 10 July 2023

Table 1. Summary of experimental parameters, measured and derived quantities for aromatic (C_xH_y) oxidation in the OFR under low-NO_x conditions.

Exp. No	VOC species	Experimental Conditions			Measured Quantities		Derived Quantities	
		VOC (ppb)	RH (%)	T (°C)	C_x HOMs (ppt)	C_{2x} HOMs (ppt)	OH_{exp} (molec cm^{-3} s)	HO_2 (ppb)
1#	benzene	110	23.6	25.0	3.4	0.4	3.1×10^{11}	1.5
2#			24.3	24.4	6.3	0.5	1.4×10^{12}	2.3
3#			24.0	25.0	6.3	0.5	1.9×10^{12}	2.4
4#			23.4	25.6	6.6	0.5	2.1×10^{12}	2.4
5#	toluene	50	29.4	23.4	3.8	0.6	3.2×10^{11}	1.5
6#			29.0	23.7	5.6	0.6	9.8×10^{11}	2.2
7#			28.3	24.3	5.0	0.5	1.5×10^{12}	2.3
8#			27.5	25.4	4.3	0.3	2.2×10^{12}	2.3
9#			26.8	26.4	3.3	0.2	2.5×10^{12}	2.2
10	m-xylene	38	26.0	23.4	8.9	3.0	2.8×10^{11}	1.5
11			27.0	23.1	14.0	3.0	9.5×10^{11}	2.2
12			24.5	24.7	10.7	2.3	1.3×10^{12}	2.4
13			24.1	24.3	9.7	2.0	1.6×10^{12}	2.4
14	1,3,5-trimethylbenzene	17	26.1	22.1	6.0	1.0	2.7×10^{11}	1.4
15			26.2	23.0	5.9	0.5	8.5×10^{11}	2.2
16			25.4	23.8	4.1	0.3	1.3×10^{12}	2.3
17			24.6	24.8	3.0	0.2	1.8×10^{12}	2.4
18			23.7	25.8	2.3	0.2	2.1×10^{12}	2.4
19#	naphthalene	12	28.7	19.5	4.2	0.3	1.2×10^{11}	0.9
20#			29.4	19.2	4.1	0.3	2.6×10^{11}	1.3
21#			28.2	20.0	4.1	0.2	7.4×10^{11}	2.0
22#			27.4	20.6	3.2	0.1	1.2×10^{12}	2.2
23#			26.6	21.5	2.8	0.1	1.6×10^{12}	2.3
24	1-methylnaphthalene	17	25.6	23.3	0.9	0.1	2.8×10^{11}	1.5
25			26.3	23.1	4.3	0.3	8.5×10^{11}	2.2
26			25.8	23.5	4.0	0.3	1.3×10^{12}	2.3
27			25.0	24.1	4.2	0.3	1.7×10^{12}	2.4

Experiments that have LTOF-SP-AMS measurements

505

https://doi.org/10.5194/egusphere-2023-1215
Preprint. Discussion started: 10 July 2023

Table 2. Rate coefficients *k* for benzene- and naphthalene-derived dimer, and comparison with data from other studies. R squares (R^2) are shown to verify the fitting results.

Dimer	R^2	$RO_2 + R'O_2$	*k* (10^{-10} cm^3 $molecule^{-1}$ s^{-1})
$C_{12}H_{14}O_{15}$	0.31	$C_6H_5O_9 + C_6H_9O_8$	3.0
		$C_6H_7O_7 + C_6H_7O_{10}$	6.4
		$C_6H_7O_8 + C_6H_7O_9$	7.0
$C_{20}H_{18}O_{14}$	0.45	$C_{10}H_5O_5 + C_{10}H_{13}O_{11}$	6.0
		$C_{10}H_5O_6 + C_{10}H_{13}O_{10}$	8.5
		$C_{10}H_5O_7 + C_{10}H_{13}O_9$	7.3
		$C_{10}H_7O_5 + C_{10}H_{11}O_{11}$	1.7
		$C_{10}H_7O_6 + C_{10}H_{11}O_{10}$	2.4
		$C_{10}H_7O_9 + C_{10}H_{11}O_7$	5.2
		$C_{10}H_7O_{11} + C_{10}H_{11}O_5$	3.9
		$C_{10}H_9O_6 + C_{10}H_9O_{10}$	1.2
		$C_{10}H_9O_8 + C_{10}H_9O_8$	0.9
$C_{18}H_{26}O_8$[a]	/	$C_9H_{13}O_5 + C_9H_{13}O_5$	1.4-2.5
$C_{20}H_{30}O_6$[b]	/	$C_{10}H_{15}O_4 + C_{10}H_{15}O_4$	0.1
$C_{20}H_{34}O_8$[b]	/	$C_{10}H_{17}O_5 + C_{10}H_{17}O_5$	0.4
$C_{20}H_{30}O_{18}$[b]	/	$C_{10}H_{15}O_{10} + C_{10}H_{15}O_{10}$	0.5
$C_{20}H_{32}O_{14}$[b]	/	$C_{10}H_{17}O_7 + C_{10}H_{15}O_9$	0.8
$C_{20}H_{30}O_{14}$[c]	/	$C_{10}H_{15}O_8 + C_{10}H_{15}O_8$	3.2
$C_{20}H_{30}O_{15}$[c]	/	$C_{10}H_{15}O_{10} + C_{10}H_{15}O_7$	8.7
		$C_{10}H_{15}O_9 + C_{10}H_{15}O_8$	6.6
$C_{20}H_{30}O_{16}$[c]	/	$C_{10}H_{15}O_{10} + C_{10}H_{15}O_8$	2.3
$C_{20}H_{30}O_{17}$[c]	/	$C_{10}H_{15}O_{11} + C_{10}H_{15}O_8$	4.4
		$C_{10}H_{15}O_{10} + C_{10}H_{15}O_9$	1.8
$C_{20}H_{30}O_{18}$[c]	/	$C_{10}H_{15}O_{12} + C_{10}H_{15}O_8$	1.6
		$C_{10}H_{15}O_{10} + C_{10}H_{15}O_{10}$	0.8

[a] from experiments with 1,3.5-trimethylbenzene addition (Berndt et al., 2018b)
[b] from experiments with α-pinene addition (Berndt et al., 2018a)
[c] from experiments with α-pinene addition (Molteni et al., 2019)